 doi:10.20944/preprints202207.0426.v1

Article

Predicting the cross-coordinated immune response dynamics in SARS-CoV-2 infection: implications for disease pathogenesis

Dmitry Grebennikov [1,2,3]*, Antonina Karsonova[3], Marina Loginova[4] , Valentina Casella[5] , Andreas Meyerhans [5,6] and Gennady Bocharov[1,2,3]*

[1] Marchuk Institute of Numerical Mathematics, Russian Academy of Sciences, Moscow, Russian Federation; dmitry.ew@gmail.com (D.G.)
[2] Moscow Center for Fundamental and Applied Mathematics at INM RAS; g.bocharov@inm.ras.ru (G.B.)
[3] Sechenov First Moscow State Medical University, Moscow, Russian Federation
[4] The National Medical Research Centre for Endocrinology of the Ministry of Healthcare of the Russian Federation, Moscow, Russian Federation
[5] Infection Biology Laboratory, Department of Medicine and Life Sciences, Universitat Pompeu Fabra, Barcelona, Spain; andreas.meyerhans@upf.edu (A.M.)
[6] Institució Catalana de Recerca i Estudis Avançats (ICREA), Barcelona, Spain
* Correspondence: dmitry.ew@gmail.com (D.G.), g.bocharov@inm.ras.ru (G.B.)

Abstract: A calibrated mathematical model of antiviral immune response to SARS-CoV-2 infection is developed. The model considers the innate and antigen-specific responses to SARS-CoV-2 infection. Recently published data sets from human challenge studies with SARS-CoV-2 were used for parameter estimation. Understanding the regulation of multiple intertwined reaction components of the immune system is necessary for linking the clinical phenotypes of COVID-19 with the kinetics of immune responses. Consideration of multiple immune reaction components in a single calibrated mathematical model allowed us to address some fundamental issues related to pathogenesis of COVID-19, i.e. sensitivity of the peak viral load to parameters characterizing the specific response components, the kinetic coordination of the individual responses, and the factors favoring a prolonged viral persistence. The model provides a tool for predicting the infectivity of patients, i.e. the amount of virus which is transmitted via droplets from the person infected with SARS-CoV-2, depending on the time of infection. The thresholds in the relative unbalance between innate and adaptive response parameters which lead to a prolonged persistence of SARS-CoV-2 due to the loss of a kinetic response synchrony/coordination were identified.

Keywords: SARS-CoV-2 infection; innate immune response; antigen-specific immune response; kinetic coordination; mathematical model; pathogenesis, long COVID-19

1. Introduction

Human infection with severe acute respiratory syndrome coronavirus 2 (SARS-CoV-2) continues to persist in the population worldwide causing the disease known as COVID-19. The time-course and severity of COVID-19 is extremely heterogenous including asymptomatic-, mild-, severe- and critical disease phenotypes [2]. Mathematical modelling is considered an important tool for understanding of pathophysiology of the SARS-CoV-2 infection via integration of multiple interactions of the virus with the human host organism [1]. The difficulties in developing relevant mathematical models of COVID-19 are due to the systemic nature of the infection, i.e. the broadness of engaged organs and physiological systems to be considered in the models, and the lack of coherent time-series data on the immune response to infection which are required to robustly calibrate the described processes. So far, more than a dozen of mathematical models of SARS-CoV-2 infection have been developed [3–14,16–21]. They differ enormously in their complexity, ranging from low-dimensional models (e.g., the ODE systems of two to five equations) [4,5,7,11,16]) through medium-size models (about ten equations) [3,6,8,13,14,17,21] up to high resolution models of ODEs (up to 60 equations) [9,10] or hybrid multi-scale models [18,20]. The later can be categorized as "experimental mathematical" models. The set of data used for the parameter estimation in the models is mainly based on similar sets of viral load kinetics

Citation: Title. *Preprints* **2022**, *1*, 0. https://doi.org/

Received:
Accepted:
Published:

 doi:10.20944/preprints202207.0426.v1

data in upper and lower respiratory tract or data from non-human primates. The biological questions addressed in the models include

- predicting the effect of therapies [4,7–10,12];
- relationship between the disease phenotype and immune response parameters [4,7,11, 13,19];
- effect of aging on disease course [7,14].

Finally, the models can be categorized according to processes considered to describe the interactions in the virus-host organism system:

- virus spreading in tissues/organs [4,7,18,19,21];
- virus spreading and innate immune responses [3,13–15];
- virus spreading and adaptive immune responses [5,6,9,11,16];
- virus spreading and innate/adaptive immune responses [8,12,17];
- virus spreading and immunophysiological responses of the host (including thrombosis, renin-angiotensin system, cytokines [10,20].

Understanding the regulation of multiple intertwined reaction components of the immune system is necessary for linking the clinical phenotypes of COVID-19 with the kinetics of the immune responses. One of the challenges is the need to understand the pathogenesis of long COVID-19. Conceptual view of the regulation of immune reactions by Grossman and Paul [24] suggests that the immune system responds to a rapid perturbation of an antigenic homeostasis. The antigenic perturbation percolates through the immune system being sequentially sensed by the innate and adaptive branches of the system. Hence, the innate (e.g., the type I interferon and inflammatory) and antigen-specific responses (CD4 T cells, CD8 T cells, B cell-mediated) need to be coordinated both in time and scale. This fundamental issue of a kinetic synchronization of innate and adaptive immune responses has not been addressed yet. The objectives of our study are

1. to develop a calibrated mathematical model of antiviral innate and adaptive immune responses to SARS-CoV-2 during mild- to-moderate symptoms infection;
2. to infer the sensitivity of the peak viral load to the kinetics of innate and adaptive responses;
3. to quantify the infectiousness of the COVID-19 patients from the onset to the recovery phase of infection;
4. to examine the effect of accelerated or decelerated components of the immune response on viral load and prolonged viral persistence;
5. to evaluate the person's infectiousness and effectiveness of testing procedures.

To proceed with the analysis of SARS-CoV-2 infection, we consider our previously developed mathematical model of antiviral immune responses [23]. Recently, it was used to infer multiplicative cooperativity of CTL and antibody responses in protection against cytopathic and non-cytopathic virus infections [25]. Originally, the model was calibrated to describe an influenza A virus infection. Both influenza A and SARS-CoV-2 are controlled by immune reactions that proceed in the system of lymph nodes draining the upper and lower respiratory tract and follow a stereotypical clonal expansion kinetics. The use of the influenza infection model as a starting point to proceed with modelling of SARS-CoV-2 infection has been shown to be useful as providing some initial parameter values [3,8,18]. Using recently published extensive data sets on the kinetics of viral load in adult humans [22] as well as some other reference data for the observed levels of CD8 T cells, antibodies and type I IFNs in serum, we refine a subset of the model parameters to reproduce the observed dynamics of the SARS-CoV-2 loads. Then, the sensitivity of the infection characteristics to model parameters is computationally studied.

In Section 2 we present the details of the mathematical model, the data used for calibration and the resulting trajectory of SARS-CoV-2 infection in terms of model characteristics. Section 3 summarizes the results of computational experiments studying the effects of variations of the process parameters on kinetics of the viral load. Finally, in Section 4 we

Preprints (www.preprints.org) | NOT PEER-REVIEWED | Posted: 27 July 2022 doi:10.20944/preprints202207.0426.v1

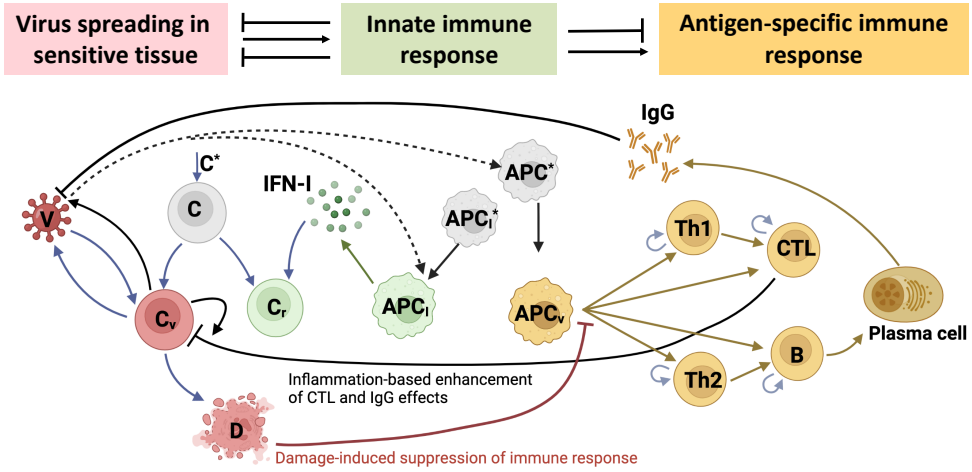

Figure 1. Biological scheme of the mathematical model of the immune response in SARS-CoV-2 infection.

discuss the implications of our analysis for SARS-CoV-2 infection (long COVID) and the coordinated regulation of immune response components.

2. Materials and Methods

2.1. Mathematical model of antiviral immune response

Mathematical model of antiviral immune response considers three major subsets of the virus-host interaction processes, i.e. the virus spreading in sensitive tissue, induction of the innate response and antigen-specific immune reactions as shown in Figure 1 and is detailed below. Consideration of innate cellular and humoral immune responses in conjunction with the infection of target organ cells and virus replication dynamics provides a tool to examine the joint impact of the considered arms of the immune system on the protection against virus infection.

2.1.1. Virus spreading in sensitive tissue

SARS-CoV-2 targets primarily the respiratory tract spreading in upper (nasal mucosa and pharynx) and lower respiratory tract (bronchi and lungs). It infects epithelial cells, ciliated airway cells, alveoli Type 2 cells [26]. The rate of change of the populations of virus-infected target cells $C_V(t)$, type I interferon protected cells $C_R(t)$, damaged target cells $D(t)$, and freely circulating virus $V(t)$ is considered to be governed by the following equations:

$$\begin{aligned}
\frac{dV}{dt}(t) &= \nu C_V(t) - (\gamma_{VC}(C^* - C_V(t) - C_R(t) - D(t)) + \\
&\quad \gamma_{VF} f_V(l) F(t) + \gamma_{VM}) V(t), && (1)\\
\frac{dC_V}{dt}(t) &= \sigma V(t)(C^* - C_V(t) - C_R(t) - D(t)) - (b_{CE} f_C(l) E(t) + b_m) C_V(t), && (2)\\
\frac{dC_R}{dt}(t) &= \sigma_R I(t)(C^* - C_V(t) - C_R(t) - D(t)) - \alpha_R C_R(t), && (3)\\
\frac{dD}{dt}(t) &= (b_{CE} f_C(l) E(t) + b_m) C_V(t) - \alpha_m D(t). && (4)
\end{aligned}$$

Preprints (www.preprints.org) | NOT PEER-REVIEWED | Posted: 27 July 2022 doi:10.20944/preprints202207.0426.v1

2.1.2. Innate immune defence reaction

The first line of reaction is related to sensing of the pathogen by the cells of the innate immune system. The innate immune response module considers the activation of professional antigen-presenting cells (including CD169 macrophages, and conventional dendritic cells, DCs) $M_V(t)$, type I Interferon (IFN) producing cells (including plasmacytoid DCs) $M_I(t)$, and type I IFN $I(t)$. The rate of changes of the concentration of these components is described by the following set of equations:

$$\frac{dM_V}{dt}(t) = \gamma_{MV} M^* V(t) - \alpha_M M_V(t), \tag{5}$$

$$\frac{dM_I}{dt}(t) = \gamma_{M_I}(M_I^* - M_I)V(t) - \alpha_{M_I} M_I(t), \tag{6}$$

$$\frac{dI}{dt}(t) = \rho_I M_I(t) - (\sigma_I(C^* - C_V(t) - C_R(t) - D(t)) + \alpha_I)I(t). \tag{7}$$

2.1.3. Antigen-specific immune response

The viral antigens processed by antigen-presenting cells activate the clones of CD4 T cells (Th1 $H_E(t)$, Th2 $H_B(t)$), CD8 T cells $E(t)$, B cells $B(t)$ resulting in the generation of plasma cells $P(t)$ and antigen-specific antibodies $F(t)$ via multiple interactions as shown in Figure 1. The respective equations of their dynamics have the structure presented below:

$$\begin{aligned}\frac{dH_E}{dt}(t) &= b_H^E(\xi(m)\rho_H^E M_V(t-\tau_H^E)H_E(t-\tau_H^E) - M_V(t)H_E(t)) \\ &\quad -b_p^{H_E} M_V(t)H_E(t)E(t) + \alpha_H^E(H_E^* - H_E(t)),\end{aligned} \tag{8}$$

$$\begin{aligned}\frac{dH_B}{dt}(t) &= b_H^B(\xi(m)\rho_H^B M_V(t-\tau_H^B)H_B(t-\tau_H^B) - M_V(t)H_B(t)) \\ &\quad -b_p^{H_B} M_V(t)H_B(t)B(t) + \alpha_H^B(H_B^* - H_B(t)),\end{aligned} \tag{9}$$

$$\begin{aligned}\frac{dE}{dt}(t) &= b_p^E(\xi(m)\rho_E M_V(t-\tau_E)H_E(t-\tau_E)E(t-\tau_E) - M_V(t)H_E(t)E(t)) \\ &\quad -b_{EC} C_V(t)E(t) + \alpha_E(E^* - E(t)),\end{aligned} \tag{10}$$

$$\begin{aligned}\frac{dB}{dt}(t) &= b_p^B(\xi(m)\rho_B M_V(t-\tau_B)H_B(t-\tau_B)B(t-\tau_B) - M_V(t)H_B(t)B(t)) \\ &\quad +\alpha_B(B^* - B(t)),\end{aligned} \tag{11}$$

$$\frac{dP}{dt}(t) = b_p^P(\xi(m)\rho_P M_V(t-\tau_P)H_B(t-\tau_P)B(t-\tau_P) + \alpha_P(P^* - P(t)), \tag{12}$$

$$\frac{dF}{dt}(t) = \rho_F P(t) - (\gamma_{FV} V(t) + \alpha_F)F(t). \tag{13}$$

2.1.4. Effects of inflammation and tissue damage

Acute infection with SARS-CoV-2 is characterized by inflammatory reactions and immune cell recruitment to the site of infection [27]. To represent this enhancing effect of elimination on the infected cells and free viruses, the following parameterizations are used

$$f_i(l) = 1 + \mu_i l, \quad i = V, C, \quad l = C_V(t)/C^*. \tag{14}$$

Finally, severe damage of the upper and lower respiratory tract suppresses the antigen-specific immune responses [28,29]. This negative feedback regulation is taken into account via the following function

$$\xi(D) = 1 - D(t)/C^*. \tag{15}$$

2.1.5. Initial conditions

The initial conditions for model equations (1-15) were defined as folows:

Preprints (www.preprints.org) | NOT PEER-REVIEWED | Posted: 27 July 2022 doi:10.20944/preprints202207.0426.v1

$$\begin{aligned} &V(0) = V_0, \quad H_E(0) = H_E^*, \quad H_B(0) = H_B^*, \quad E(0) = E^*, \\ &B(0) = B^*, \quad P(0) = P^*, \quad F(0) = F^*, \\ &C_V(0) = 0, \quad C_R(0) = 0, \quad D(0) = 0, \quad M_V(0) = 0, \quad M_I(0) = 0, \quad I(0) = 0, \end{aligned} \tag{16}$$

where V_0 is the initial viral load in the upper respiratory tract, H_E^*, H_B^*, E^* and B^* are homeostatic concentrations for antigen-specific Th1, Th2, CTL and B cells in the lung-draining LNs, P^* and F^* are homeostatic concentrations for antigen-specific plasma cells and antibodies in blood, respectively. We assume no immune activation is present before the moment of infection:

$$M_V(t) = 0, \quad t < 0. \tag{17}$$

2.2. Reference data on SARS-CoV-2 infection

In our study, we used recent data on viral kinetics during SARS-CoV-2 human challenge in young adults [22]. The data provide a most detailed characterization of the viral load (copies per ml) in nose and throat of the adult volunteers. In addition, we considered the data on the serum levels of IFN [32], the virus-specific Abs and the CD8 T cells [31]. The data are shown either as mean +/- sem (viral load in nose), or some shadowed areas in Figure 2.

2.3. Calibration of the model

The estimate for initial viral load V_0 can be derived from the experimental data on viral load [22] which we aim to reproduce. The participants were inocculated intranasally with the dose of 10 $\text{TCID}_{50} \approx 7$ PFU of SARS-CoV-2. To obtain the initial concentration V_0, we estimate the volume of nasal mucosa as $120 - 150$ cm^2 of surface area times the thickness of $0.3 - 5$ mm [39,40]. This gives us the range of values from 3.6 to 75 ml, with 7 ml being a harmonic mean. Thus, we fix $V_0 \approx 7$ PFU/7 ml$= 1$ virion/ml. Note that more thorough estimates for infection dose and model parameters affecting the incubation period dynamics should be obtained using discrete-state stochastic models.

The homeostatic concentrations H_E^*, H_B^*, E^*, B^* are estimated as follows: the frequency of antigen-specific cells is about $10^{-7} - 10^{-4}$ [33–36], there are about 2×10^{11} immune cells of each type totally in approximately 1 litre of lymphoid tissue of the organism [37], the volume of the lung-draining lymphoid tissue is about 10 ml (=1%) [23], which gives the range $(10^{-7}, 10^{-4}) \times 2 \times 10^{11} \times 0.01/10 = (20, 20000)$ cells/ml. We use the geometric mean of around 600 cells/ml for the point estimate. The estimates for P^* and F^* are borrowed from [23].

The calibration procedure consists of three stages: (i) deriving the estimates for admissible ranges and initial guesses of model parameters based on available literature, (ii) choosing a subset of parameters having a large effect on discrepancy between model solution and data based on sensitivity analysis, (iii) tuning parameters from a chosen subset in specified ranges to obtain an overall good fit, (iv) final refinement of parameters by solving a local nonlinear optimization problem to minimize the specified discrepancy.

The measure of discrepancy to be minimized is defined as

$$\Phi(p) = \sum_{j=1}^{M} \left[\left(\frac{V(t_j, p) - V_j^{obs}}{V_j^{obs}} \right)^2 + \left(\frac{V(t_j, p) - V_j^{obs}}{V(t_j, p)} \right)^2 \right], \tag{18}$$

where $V(t_j, p)$ is the viral load predicted by the model with parameter values p at M time points t_j, V_j^{obs} is the experimental data on viral load at corresponding time points. This functional weighs similarly both deviations at high and low viral load values [23].

Preprints (www.preprints.org) | NOT PEER-REVIEWED | Posted: 27 July 2022 doi:10.20944/preprints202207.0426.v1

As a starting point, we used the parameter values and ranges specified in the previously calibrated model of influenza A virus infection [23,25]. Some parameter estimates were refined, as described below.

To determine a subset of parameters to variate, we analyzed the sensitivity of parameters towards the partial sums of functional (18) at certain time points, corresponding to different stages of infection (see section 2.4). We can select the following parameters as having the most effect on each stage:

- First stage (incubation period, 0-3 days): $\nu, \sigma, \gamma_{VC}, \gamma_{VM}$.
- Second stage (activation of immune response and peak of viral load, 4-7 days) and third stage (recovery period, 8-13 days): $\sigma_R, \rho_I, \gamma_{VF}, \gamma_{FV}, \sigma_I, \mu_V, \gamma_{M_I}, b_p^P, \gamma_{MV}$.
- Forth stage (post-symptomatic period, 14-19 days): $b_{CE}, \gamma_{VC}, b_H^B$.

Note that some parameters naturally have influence on several stages. However, one can derive a good fit by sequentially tuning the subsets of parameters for each stage. Also, the parameters reported above don't include parameters for which we already have a good estimate and narrow ranges from [23].

For the rate of SARS-CoV-2 virions secretion per infected epithelial cell, ν, we set the initial guess $\nu = 130$ day^{-1} and admissible range $(10, 1000)$ day^{-1} based on our previous experience of modelling SARS-CoV-2 replication cycle [30,38].

The infection rate of target epithelial cells with SARS-CoV-2, σ, can be estimated as $\sigma \approx 1/(t_{l.c.} \times V_{MOI} \times f_D \times C^*)$, where $t_{l.c.}$ is a typical duration of the intracellular replication cycle, V_{MOI} is a multiplicity of single cell infection, and f_D is a fraction of epithelial cells in lungs damaged during infection [23]. Taking the ranges $t_{l.c.} \in (7, 24)$ h, $V_{MOI} \in (1, 10)$ [30,38], and $f_D \in (0.1, 0.5)$, $C^* \in (10^9, 10^{10})$ cells [23], we arrive to the estimate $\sigma \in (2 \times 10^{-11}, 3 \times 10^{-8})$ (cells/ml)$^{-1}$day^{-1}.

The expenditure rate of virions on the infection of target cells, γ_{VC}, should be balanced with the infection rate σ. These parameters can be related through $\gamma_{VC} = V_{MOI} \times \sigma$, where V_{MOI} is the number of virions infecting a single target cell, for which we set the initial guess and the range $V_{MOI} = 10 \in (1, 20)$.

The rate of CTL-mediated destruction of epithelial cells, b_{CE}, can be estimated using the scheme suggested in [23]: $b_{CE} \approx 1/(t_{LN \to RT} \times E_{suf})$. Here, E_{suf} is the number of CTLs sufficient to destroy $f_D \times C^*$ epithelial cells, and $t_{LN \to RT} \in (2, 12)$ h is the typical time for a CTL to reach the target compartment of respiratory tract mucosa from LNs draining the lungs. As one CTL can destroy several target cells (≈ 10), the estimate is $b_{CE} \in (4 \times 10^{-9}, 4 \times 10^{-7})$ (virions/ml)$^{-1}$day^{-1}.

We used the estimates as initial guesses and ranges from [23] for parameters $\gamma_{VM}, \gamma_{M_I}, \sigma_R, \sigma_I, \gamma_V$

Preprints (www.preprints.org) | NOT PEER-REVIEWED | Posted: 27 July 2022 doi:10.20944/preprints202207.0426.v1

Table 1. Parameters of the calibrated model.

	Parameter, units	Range, initial guess	Estimate
M^*	Concentration of APCs, cells/ml	$(3 \times 10^5, 2 \times 10^6)$	6×10^5
M_I^*	Concentration of IFN-producing APCs, cells/ml	$(10^7, 10^9)$	10^9
H_E^*	Concentration of SARS-CoV-2 specific Th1 cells, cells/ml	$(20, 20000)$	600
H_B^*	Concentration of SARS-CoV-2 specific Th2 cells, cells/ml	$(20, 20000)$	600
E^*	Concentration of SARS-CoV-2 specific CTLs, cells/ml	$(20, 20000)$	600
B^*	Concentration of SARS-CoV-2 specific B cells, cells/ml	$(20, 20000)$	600
P^*	Concentration of SARS-CoV-2 specific plasma cells, cells/ml	$(2, 42)$	10
F^*	Concentration of SARS-CoV-2 specific antibodies, molecules/ml	$(10^7, 10^8)$	5×10^7
C^*	Concentration of epithelial cells, cells/ml	$(10^9, 10^{10})$	10^{10}
α_M	Rate of stimulated state loss for APCs, day^{-1}	$(1, 3.3)$	3.3
α_H^E	Rate of activated state loss for Th1 cells, day^{-1}	$(0.8, 1.2)$	1
α_H^B	Rate of activated state loss for Th2 cells, day^{-1}	$(0.8, 1.2)$	1
α_E	Rate of natural death for CTLs, day^{-1}	$(0.33, 0.5)$	0.4
α_B	Rate of natural death for B cells, day^{-1}	$(0.05, 0.1)$	0.1
α_P	Rate of natural death for plasma cells, day^{-1}	$(0.33, 0.5)$	0.4
α_F	Rate of natural death for antibodies, day^{-1}	0.043	0.043
τ_H^E	Duration of Th1 cell division cycle, days	$(0.4, 0.8)$	0.6
τ_H^B	Duration of Th2 cell division cycle, days	$(0.4, 0.8)$	0.6
τ_E	Duration of CTL division cycle, days	$(0.5, 1)$	0.5
τ_B	Duration of B cell division cycle, days	$(0.5, 1)$	0.5
τ_P	Duration of B cell differentiation into plasma cells, days	$(0.5, 1)$	0.5
ρ_H^E	Number of Th1 cells created during division cycle	$(2, 4)$	4
ρ_H^B	Number of Th2 cells created during division cycle	$(2, 4)$	4
ρ_E	Number of CTLs created during division cycle	$(2, 4)$	2
ρ_B	Number of B cells in clone created by series of 1 or 2 divisions	$(1.5, 3)$	3
ρ_P	Number of plasma cells in clone created by series of 1 or 2 divisions	$(0.5, 1)$	1
ρ_F	Rate of IgG production per plasma cell, molecules/cell/day	$(8.5 \times 10^5, 1.7 \times 10^6)$	1.7×10^6
b_H^E	Rate of Th1 cells stimulation, $(\text{cells/ml})^{-1}\text{day}^{-1}$	$(5 \times 10^{-7}, 4.5 \times 10^{-4})$	4.5×10^{-5}
b_H^B	Rate of Th2 cells stimulation, $(\text{cells/ml})^{-1}\text{day}^{-1}$	$(5 \times 10^{-7}, 4.5 \times 10^{-4})$	4.5×10^{-5}
b_p^E	Rate of CTL stimulation, $(\text{cells/ml})^{-2}\text{day}^{-1}$	$(1.4 \times 10^{-10}, 2 \times 10^{-8})$	1.4×10^{-8}
b_p^B	Rate of B cell stimulation, $(\text{cells/ml})^{-2}\text{day}^{-1}$	$(1.4 \times 10^{-10}, 3 \times 10^{-9})$	2.2×10^{-9}
b_p^P	Rate of plasma cell stimulation, $(\text{cells/ml})^{-2}\text{day}^{-1}$	$(1.4 \times 10^{-10}, 3 \times 10^{-9}), 2.2 \times 10^{-9}$	3×10^{-9}
$b_p^{H_E}$	Rate of Th1 cells suppression, $(\text{cells/ml})^{-2}\text{day}^{-1}$	-	2.8×10^{-13}
$b_p^{H_B}$	Rate of Th2 cells suppression, $(\text{cells/ml})^{-2}\text{day}^{-1}$	-	2.8×10^{-13}
γ_{MV}	Rate of APC stimulation, $(\text{cells/ml})^{-1}\text{day}^{-1}$	$(1.7 \times 10^{-13}, 10^{-7}), 2 \times 10^{-6}$	1.9×10^{-9}
γ_{FV}	Rate of IgG binding to SARS-CoV-2, $(\text{virions/ml})^{-1}\text{day}^{-1}$	$(1.4 \times 10^{-10}, 1.4 \times 10^{-8}), 1.4 \times 10^{-9}$	2.8×10^{-9}
σ	Rate of epithelial cell infection with SARS-CoV-2, $(\text{cells/ml})^{-1}\text{day}^{-1}$	$(2 \times 10^{-11}, 3 \times 10^{-8}), 10^{-10}$	1.4×10^{-10}
b_{CE}	Rate of infected epithelial cell damage by CTLs, $(\text{virions/ml})^{-1}\text{day}^{-1}$	$(4 \times 10^{-9}, 4 \times 10^{-7}), 5 \times 10^{-8}$	4×10^{-9}
b_{EC}	Rate of CTL death due to lytic interactions with infected cells, $(\text{cells/ml})^{-1}\text{day}^{-1}$	-	2.7×10^{-10}
b_m	Rate of infected cell damage due to SARS-CoV-2 cytopathicity, day^{-1}	$(0.5, 2)$	1.5
α_m	Rate of epithelial cell regeneration, day^{-1}	$(1, 4)$	4
ν	Rate of SARS-CoV-2 virions secretion per infected epithelial cell, day^{-1}	$(10, 10^4), 130$	144
γ_{VC}	Rate of SARS-CoV-2 absorption by epithelial cell, $(\text{cells/ml})^{-1}\text{day}^{-1}$	$(2 \times 10^{-11}, 6 \times 10^{-7}), 10^{-9}$	3.2×10^{-9}
γ_{VM}	Rate of nonspecific SARS-CoV-2 elimination, day^{-1}	$(2, 4), 1.7$	4
γ_{VF}	Rate of SARS-CoV-2 neutralization by specific IgG, $(\text{virions/ml})^{-1}\text{day}^{-1}$	$(1.4 \times 10^{-11}, 1.4 \times 10^{-8}), 1.4 \times 10^{-9}$	1.4×10^{-8}
μ_V	Parameter for inflamation-based enhancement of IgG effect	$(10, 10^5), 1000$	2628
μ_C	Parameter for inflamation-based enhancement of CTL effect	$(10, 10^5), 1000$	1407
γ_{M_I}	Rate of induction of IFN-producing state in APCs, $(\text{cells/ml})^{-1}\text{day}^{-1}$	$(2.3 \times 10^{-9}, 2.3 \times 10^{-7}), 1.7 \times 10^{-8}$	5.7×10^{-8}
α_{M_I}	Rate of IFN-producing state loss by APCs, day^{-1}	$(0.3, 0.5)$	0.5
ρ_I	Rate of IFN production per IFN-producing cells, molecules/cell/day	$(500, 12000)$	6000
α_I	Type I IFN clearance rate, day^{-1}	$(10, 100)$	24
σ_I	Rate of IFN binding with epithelial cells, $(\text{cells/ml})^{-1}\text{day}^{-1}$	$(1.7 \times 10^{-11}, 1.7 \times 10^{-9}), 1.7 \times 10^{-9}$	1.7×10^{-11}
σ_R	Rate of virus-resistant state induction in epithelial cells, $(\text{cells/ml})^{-1}\text{day}^{-1}$	$(3.3 \times 10^{-12}, 3.3 \times 10^{-10}), 3.3 \times 10^{-11}$	9.9×10^{-11}
α_R	Rate of virus-resistant state loss in epithelial cells, day^{-1}	-	1

Preprints (www.preprints.org) | NOT PEER-REVIEWED | Posted: 27 July 2022 doi:10.20944/preprints202207.0426.v1

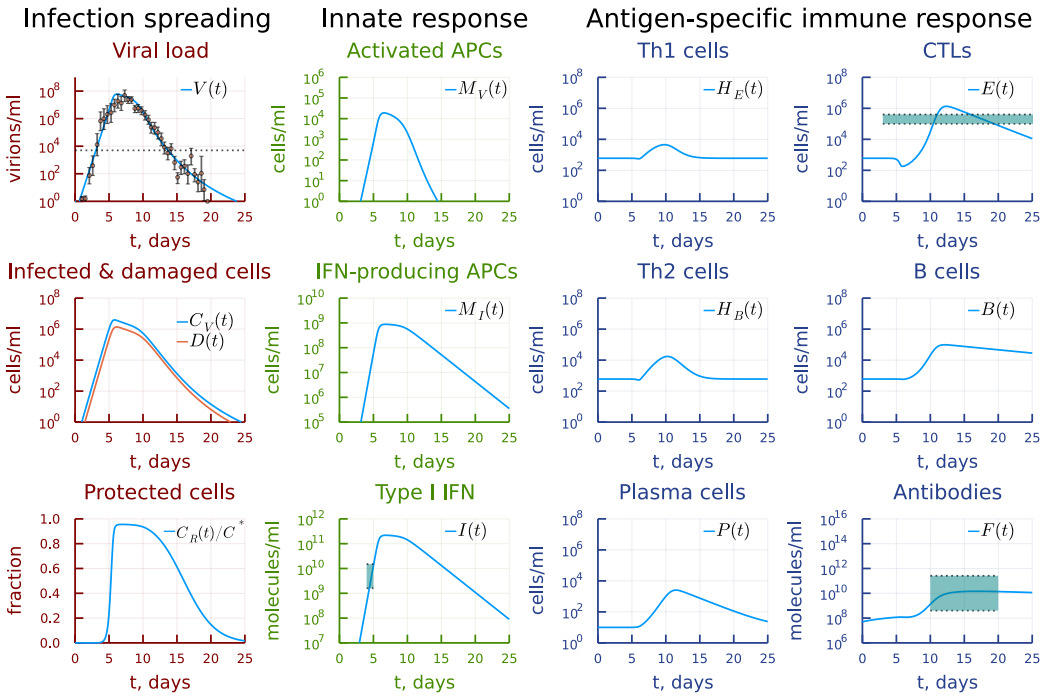

Figure 2. Baseline solution of the model describing the intra-host SARS-CoV-2 infection dynamics and the available clinical data.

The remaining model parameters were not varied; instead, their values were fixed to the estimates from [23]. Note that concentrations are reported in Table 1 as numbers of cells, virions or molecules per ml as opposed to molar units used in the previous work.

For final stage of calibration we numerically solved a problem of minimizing (18) with respect to parameters, using a local method. We used first the derivative-free Nelder-Mead method, followed by the derivative-based quasi-Newton L-BGFS method using the meta-package Optimization.jl in julia language.

The final estimates of calibrated model parameters p are presented in Table 1. Initial guess is reported only for parameters which were tuned during the calibration process. The calibrated model parameters correspond to discrepancy $\Phi(p) = 1086$. The baseline solution of the model describing the intra-host SARS-CoV-2 infection and antiviral immune response dynamics and the available clinical data are shown in Figure 2.

2.4. Sensitivity analysis

Sensitivity analysis was employed both as exploratory tool in the calibration process, and as a way to derive meaningful predictions of the calibrated model. We used a local sensitivity approach, in which sensitivity indices of some functional of the model solution $\Phi(y(p))$ with respect to variations in model parameters p_j are defined as

$$s_j = \frac{d\Phi}{dp_j}(p), \quad \hat{s}_j = p_j s_j, \tag{19}$$

and provide a measure of the influence of parameter variations on the functional. The normalized version $\hat{s}_j$ of sensitivity indices provides the way to compare and rank the parameters based on their effect.

We used the following functionals of interest in this work:

$$\Phi_{AUC} = \int_0^T V(t)dt, \quad \Phi_{peak} = \max_{t\in[0,T]}(V(t)), \tag{20}$$

Preprints (www.preprints.org) | NOT PEER-REVIEWED | Posted: 27 July 2022 doi:10.20944/preprints202207.0426.v1

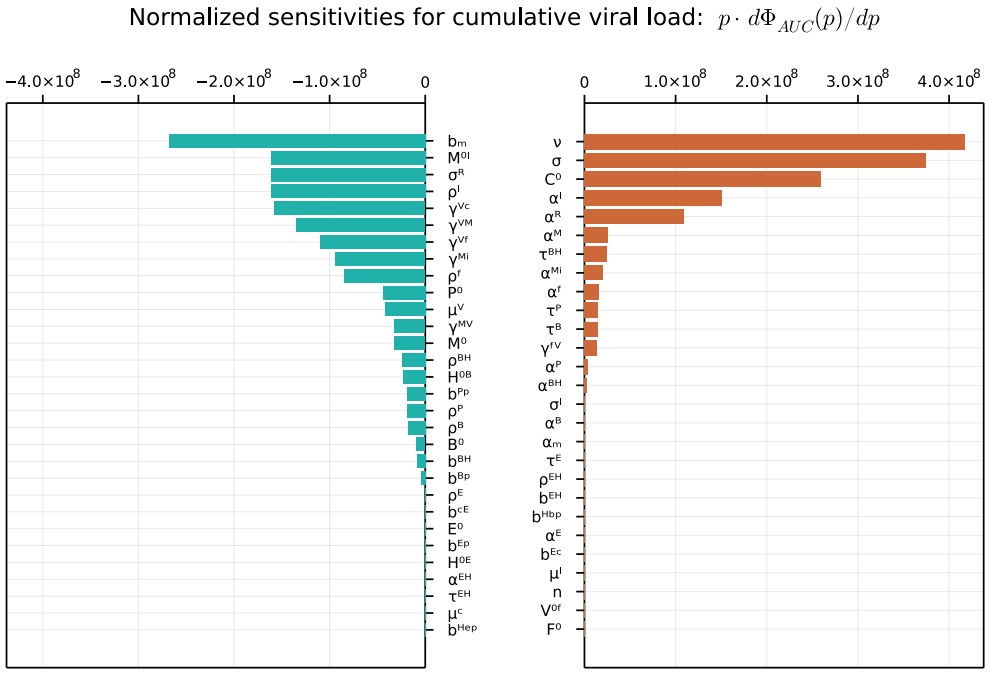

Figure 3. Normalized sensitivity indices for cumulative viral load $\Phi_{AUC}(p) = 1.6 \times 10^8$.

where Φ_{AUC} refers to the cumulative viral load during the time course of infection, Φ_{peak} is the peak viral load. Additionally, we analyzed sensitivity of the functional of discrepancy with experimental data (18) at various subsets of time points during the calibration process.

All sensitivity indices were calculated using forward-mode automatic differentiation available in the package ForwardDiff.jl in julia language.

3. Results

3.1. Local sensitivity analysis

The sensitivity analysis of the cumulative viral load, which is an important characteristic affecting positive and negative the dynamics of immune responses [42], showed a strong positive dependence on the virus secretion rate, the target cell infection rate and the number of available target cells expressing ACE2. It is most strongly negatively affected by the parameter of innate immune response related to activation of APCs and type I IFN system as summarized in Figure 3. The peak viral load has a similar sensitivity ranking with respect to the most influential parameters, see Figure 4.

3.2. Induction of antigen-presenting cells

The cascade of antiviral immune responses starts with activation of antigen presenting cells. The sensitivity threshold is characterized by model parameter γ_{MV}. We examined the effect of its 10-times increase and decrease on the course of the virus infection as shown in Figure 5. The model predicts that a higher sensitivity induces faster and stronger responses which spread through the whole response cascade. However, a ten-fold decrease results in higher viral antigen levels which are needed to induce activate the immune system, which delays the immune response and finally, favours prolonged viral persistence. Interestingly, that a stronger type I IFN response is not sufficient to clear the infection in this case.

3.3. Induction of type I IFN response

The ten-fold increase of the rate constant of activation of type I IFN response γ_{M_I} results in a lower viral peak as one can see in Figure 6. However, this affect the activation of antigen-presenting cells and the resulting reduced response percolates through to antigen-specific arms. Both the T-cell and B-cell responses appear to be weaker. The virus is not

Preprints (www.preprints.org) | NOT PEER-REVIEWED | Posted: 27 July 2022 doi:10.20944/preprints202207.0426.v1

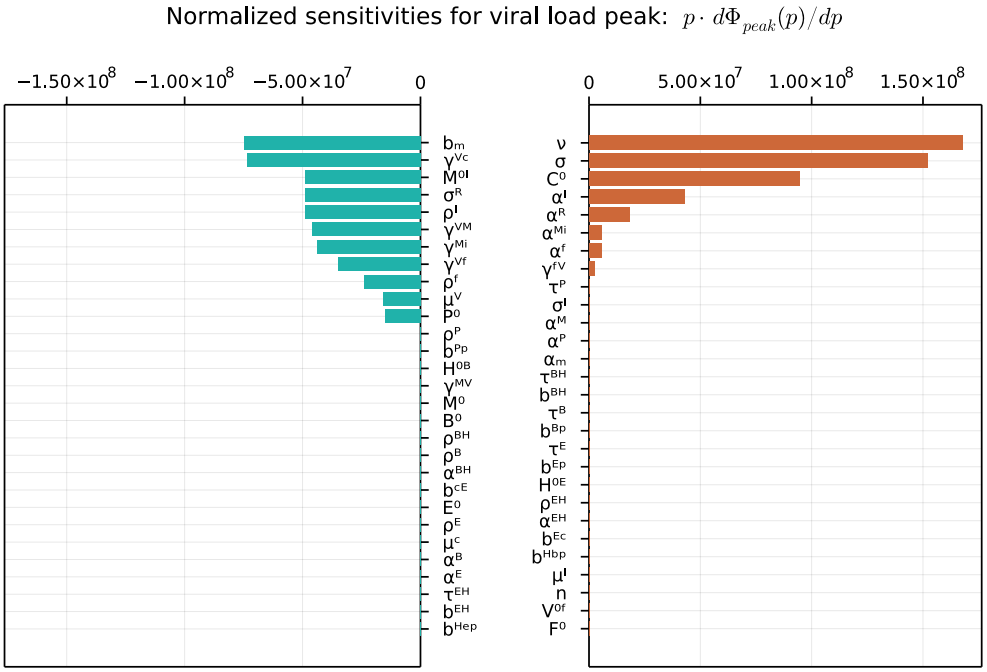

Figure 4. Normalized sensitivity indices for viral load peak $\Phi_{peak}(p) = 5.9 \times 10^7$.

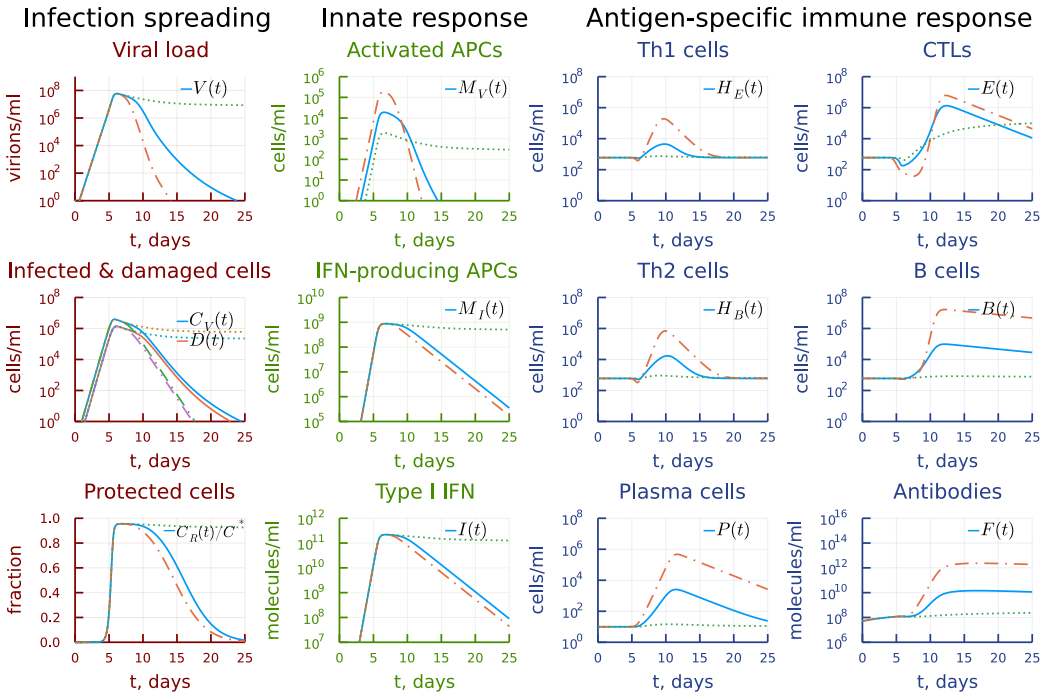

Figure 5. Dashdot: 10-fold increase of γ_{MV}, dot: 10-fold decrease of γ_{MV} relative to baseline value.

Preprints (www.preprints.org) | NOT PEER-REVIEWED | Posted: 27 July 2022 doi:10.20944/preprints202207.0426.v1

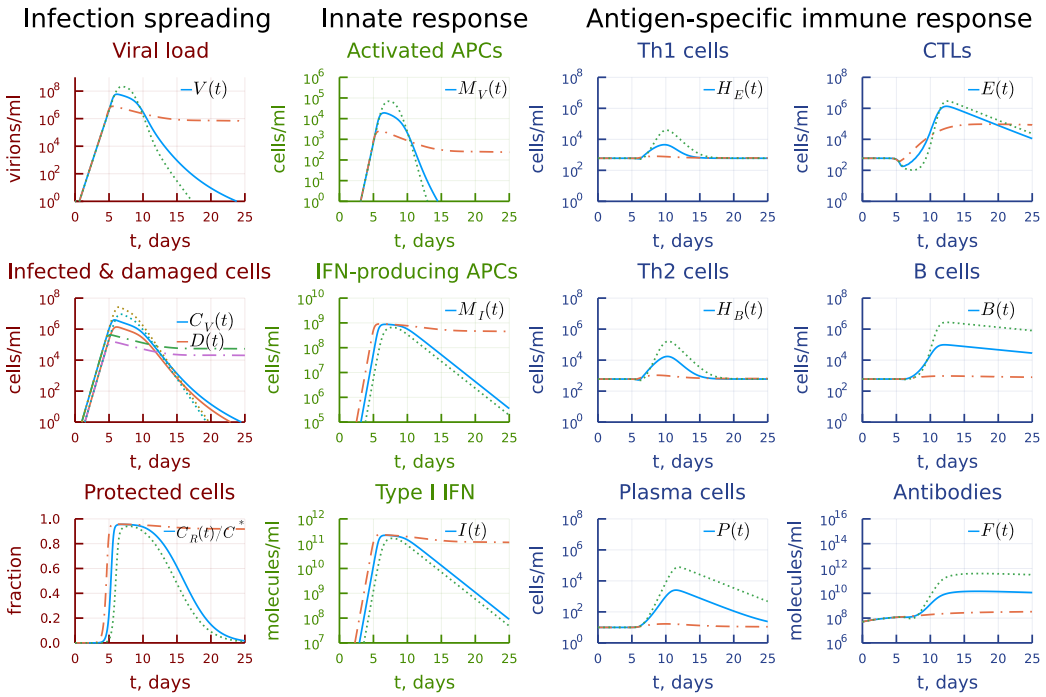

Figure 6. Dashdot: 10-fold increase of γ_{M_I}, dot: 10-fold decrease of γ_{M_I} relative to baseline value.

eliminated within 25 days so that the viral persistence is observed. A similar decrease in γ_{M_I} leads to a poorer control of viral load so that it reaches higher peaks. The antigen specific-response turn out to be stronger. However, the damage of the target organs also increases by one order of maginitude.

The effect of 10-fold variation of the parameter σ_R characterizing the rate of type I IFN-mediated induction of resistance to infection of target cells expressing ACE2 is displayed in Figure 7. Its impact on the solution of the model is similar to that of γ_{M_I}.

3.4. Disregulation of CTL and B-cell responses

Next, we examined the extent of kinetic cooperativity between the T- and B cell responses. To this end, a 10-fold variation was applied to parameter b_p^B, clonal activation rate of B cells. The results are summarized in Figure 8. An earlier activation of the humoral immune response results in faster (by 5 days) viral elimination but reduces the CTL response. A delayed activation of B cells critically affects the dynamics of infection resulting in a prolonger viral persistence.

A similar exploration of the effect of two-fold increasing the activation rate of CTL clonal expansion at the background of an opposite two-fold variation of the activation rate of B cells is shown in Figure 9. The increase in CTL response turns out to be much stronger but it fails to eliminate the infection because the humoral immune response is not sufficient. The effect of the reduced activation rate of CTL response can be compensated by a two-fold increase of the activation rate of B cells, so that the infection is completely eliminated.

The 10-fold increase of the differentiation rate of antigen-specific B cells into plasma cells b_p^P leads to an earlier appearance of antibodies as displayed in Figure 10. However, the clonal expansion of B cells and CTL is smaller which finally results in failure of the system to eliminate the virus. Reduced differentiation rate slightly increases the duration of the peak viral load but a stronger B- and T cell responses finally eliminate the virus infection five days earlier compared to the basal solution pattern.

A higher extent of variation of the differentiation rate of B cells into plasma cells (i.e., by 40-times) changes the dynamics as shown in Figures 11. The respective increase results in sufficient production of antibodies eliminating the virus. However, the cumulative viral load is smaller and hence, the expansion of T cells and B cells. The decrease of the

Preprints (www.preprints.org) | NOT PEER-REVIEWED | Posted: 27 July 2022 doi:10.20944/preprints202207.0426.v1

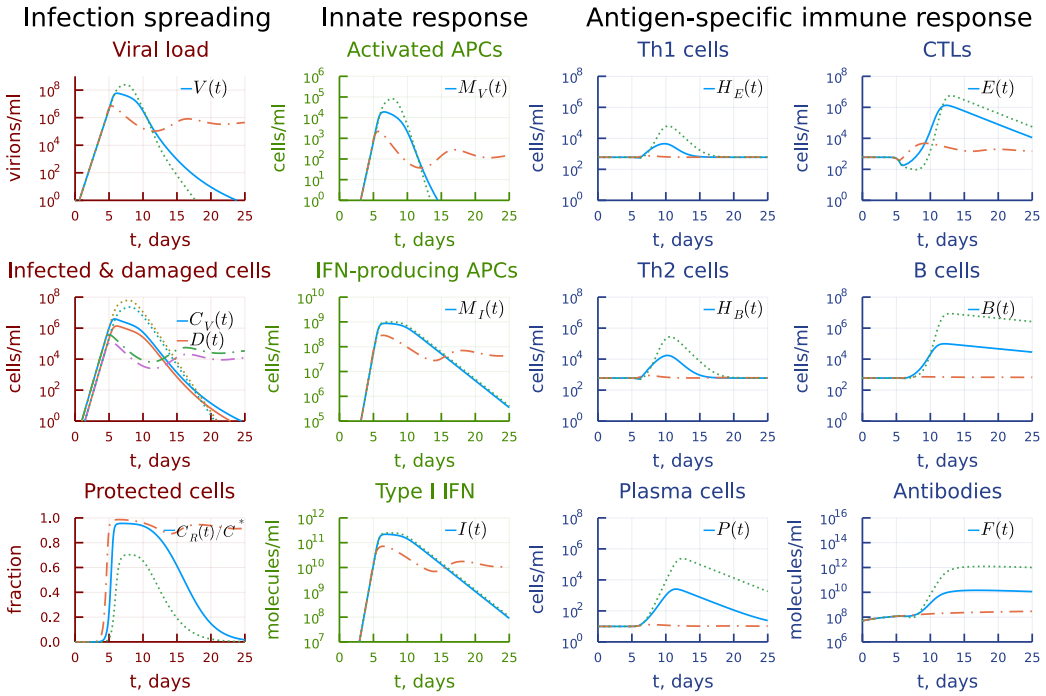

Figure 7. Dashdot: 10-fold increase of σ_R, dot: 10-fold decrease of σ_R relative to baseline value.

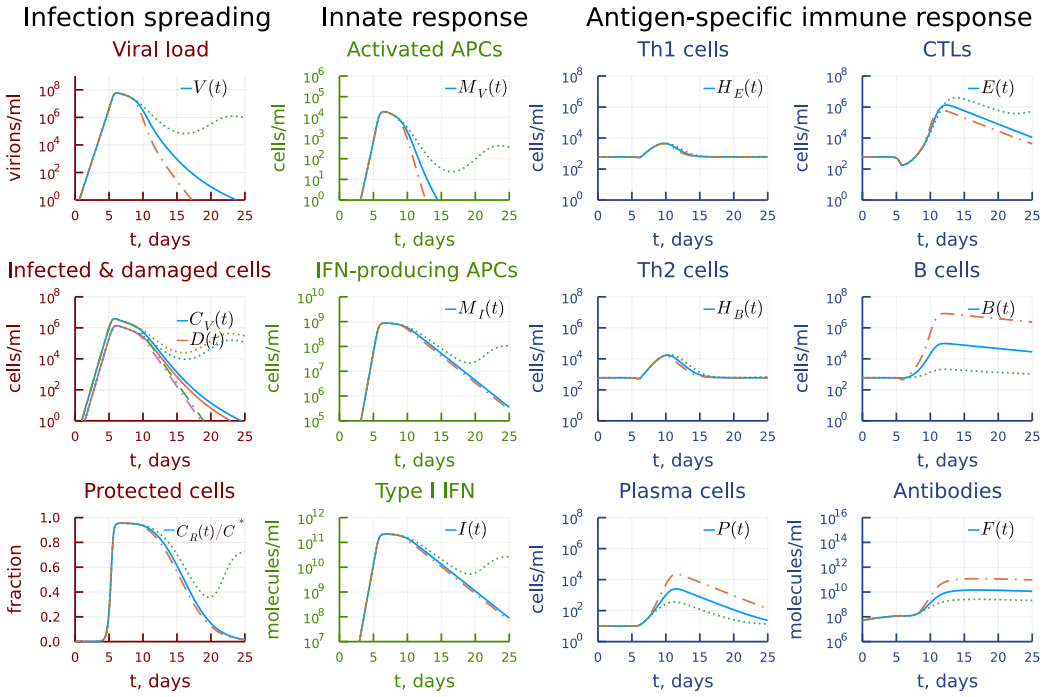

Figure 8. Dashdot: 10-fold increase of b_p^B, dot: 10-fold decrease of b_p^B relative to baseline value.

Preprints (www.preprints.org) | NOT PEER-REVIEWED | Posted: 27 July 2022 doi:10.20944/preprints202207.0426.v1

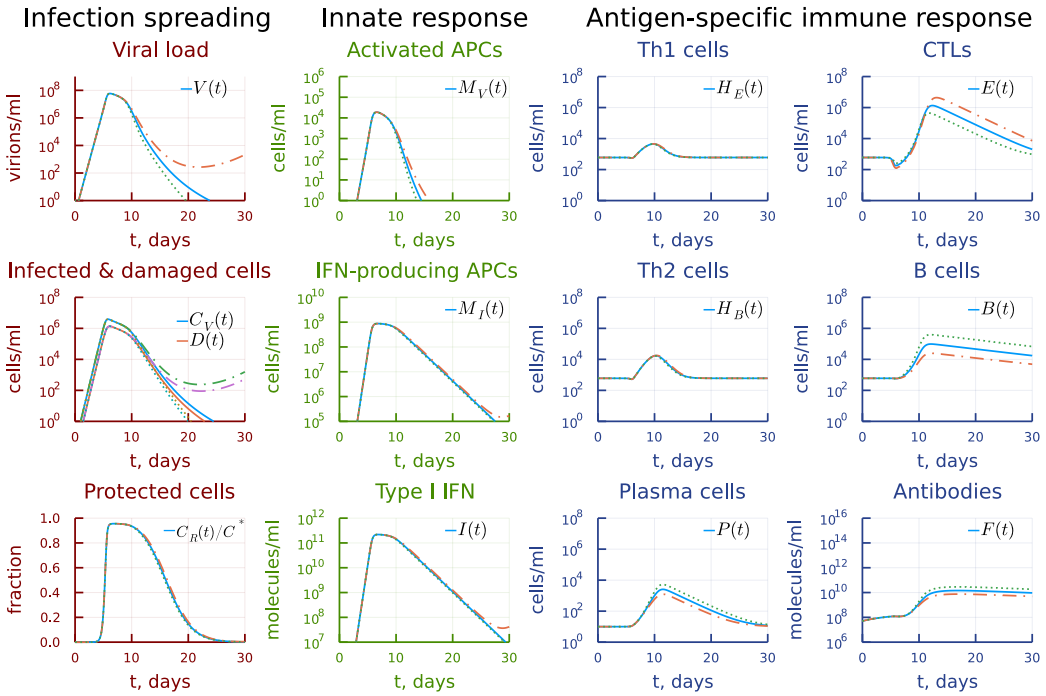

Figure 9. Dashdot: 2-fold increase of b_p^E with 2-fold decrease of b_p^B, dot: 2-fold decrease of b_p^E with 2-fold increase of b_p^B relative to baseline value.

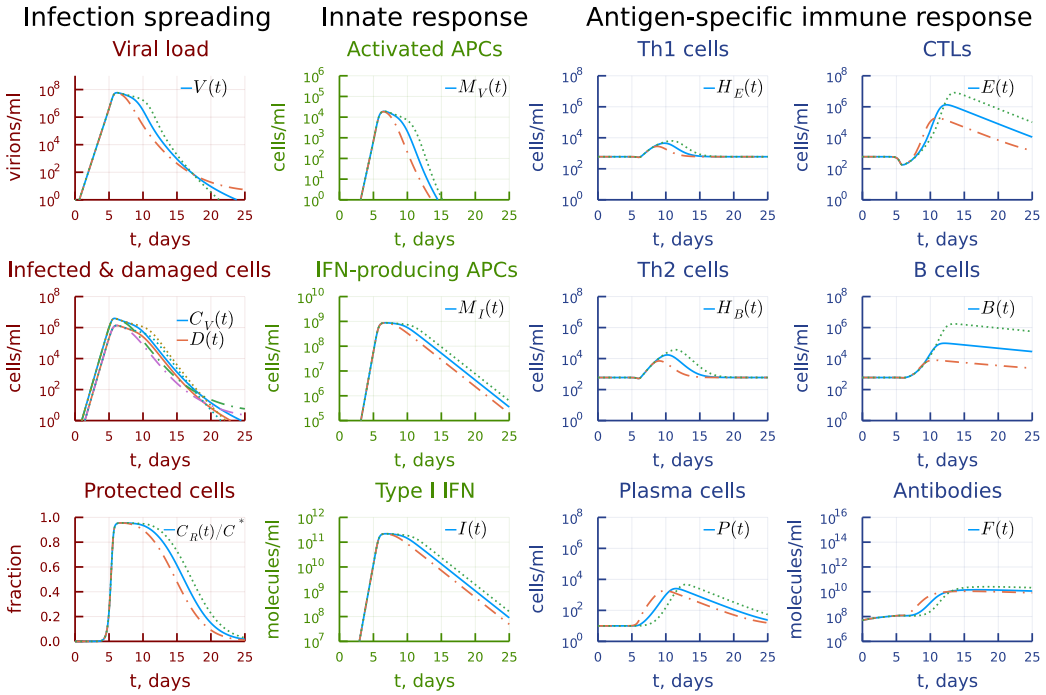

Figure 10. Dashdot: 10-fold increase of b_p^P, dot: 10-fold decrease of b_p^P relative to baseline value.

Preprints (www.preprints.org) | NOT PEER-REVIEWED | Posted: 27 July 2022 doi:10.20944/preprints202207.0426.v1

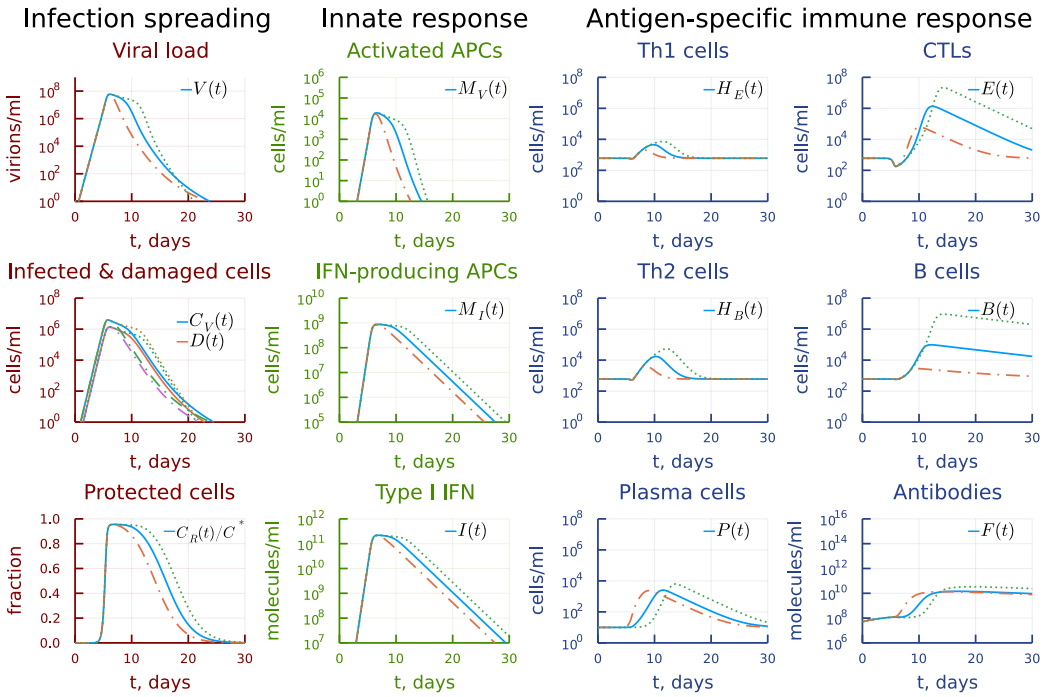

Figure 11. Dashdot: 40-fold increase of b_p^P, dot: 40-fold decrease of b_p^P relative to baseline value.

differentiation rate of B cells into plasma cells results in an delayed but enhanced Th1, Th2, CTL and B cell and plasma cell expansion. This solution trajectory is characterized by a higher number of damaged infected target cells and prolonged viral persistence at the peak levels.

3.5. Asymmetry of Th1 versus Th2 responses

It has been recently observed that epidemiological data indicate a reduced risk of severe COVID-19 in SARS-CoV-2 infected patients with the type 2 asthma [41]. Asthma is considered to be associated with a dominance of T helper 2 (Th2) cells. We used the model to predict the impact of a stronger activation rate of Th2 cells b_H^B compared to Th1 cells on the dynamics of infection. The results are presented in Figure 12. The ten-fold increase of the clonal expansion rate of Th2 cells leads to an earlier elimination of virus due to enhanced (by several orders or magnitude) humoral immune response, with the CTL response left almost unchanged. However, a similar reduction in the activation rate essentially reduced all components of the B-cell and antibody responses. The stronger induction of CTL response is not enough to compensate the weaker humoral immune response and the prolonged viral persistence is predicted.

The biased towards Th2 cells antigen-specific immune response could also be a consequence of a larger homeostatic number of this population compared to Th1 cells. Figure 13 shows the effect of a five-times variation of the respective parameter H_B^*. A higher initial number of SARS-CoV-2-specific Th2 cells leads to an earlier and stronger B-cell response and faster virus elimination. Similar reduction results in a delayed CTL and B-cell responses and prolonged viral persistence.

3.6. Kinetic mechanisms of long COVID-19 pathogenesis

Following the above examination of the degree of synchrony in the cascade of antiviral immune response, we estimated the degree of variation in the respective parameters which lead to prolonged viral persistence, i.e. beyond 30 days post infection. The results are summarized in Table 2.

Preprints (www.preprints.org) | NOT PEER-REVIEWED | Posted: 27 July 2022 doi:10.20944/preprints202207.0426.v1

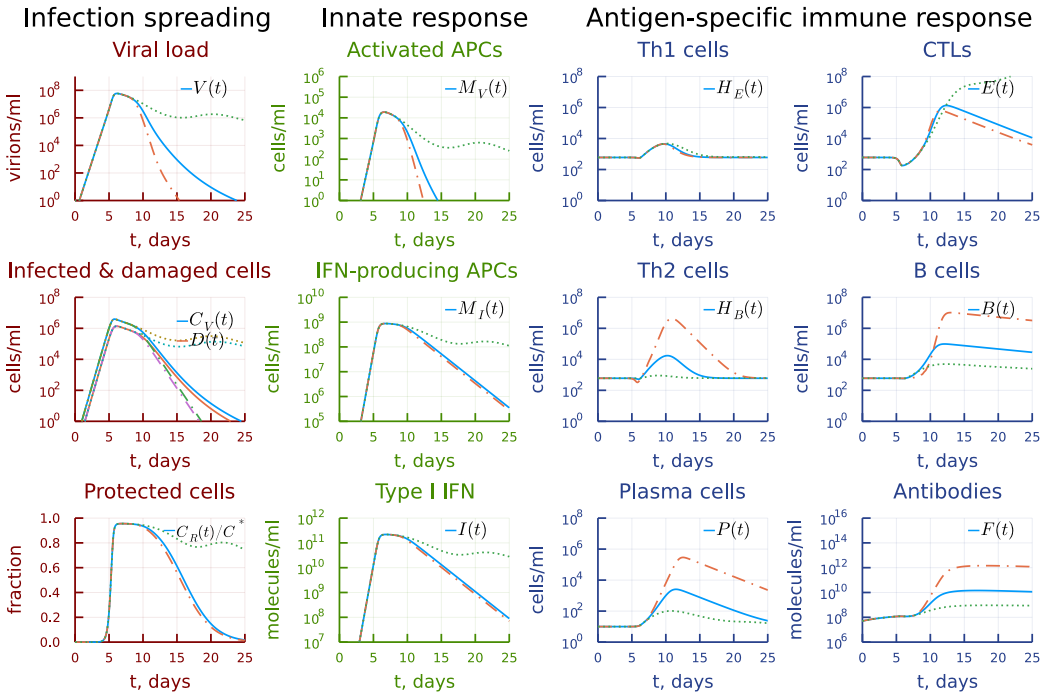

Figure 12. Dashdot: 10-fold increase of b_H^B, dot: 10-fold decrease of b_H^B relative to baseline value.

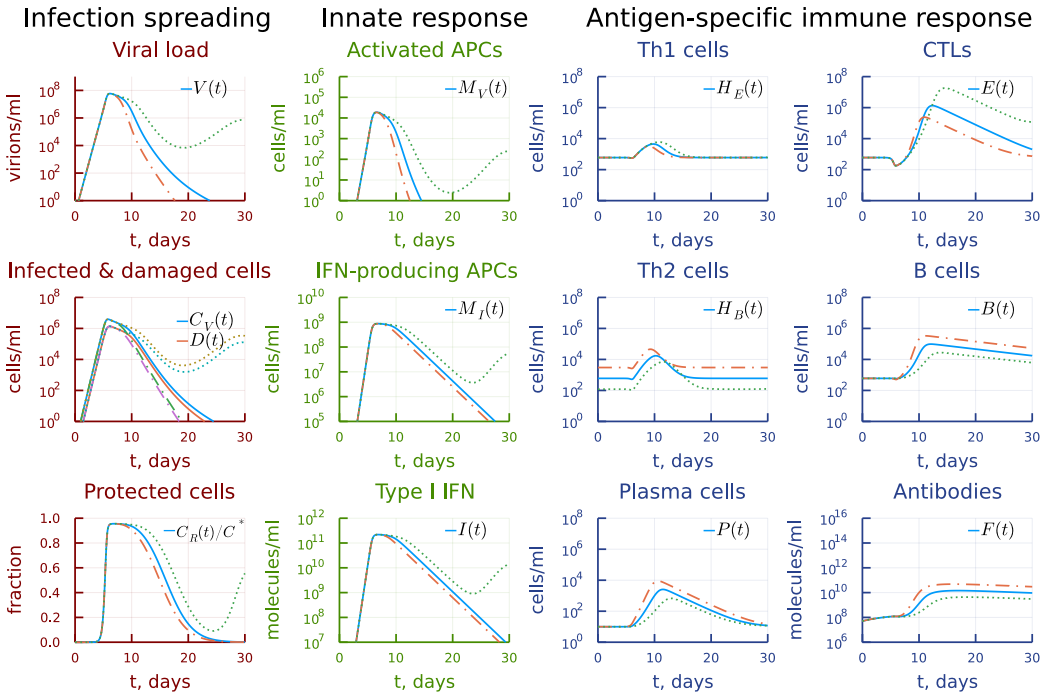

Figure 13. Dashdot: 5-fold increase of H_B^*, dot: 5-fold decrease of H_B^* relative to baseline value.

Preprints (www.preprints.org) | NOT PEER-REVIEWED | Posted: 27 July 2022 doi:10.20944/preprints202207.0426.v1

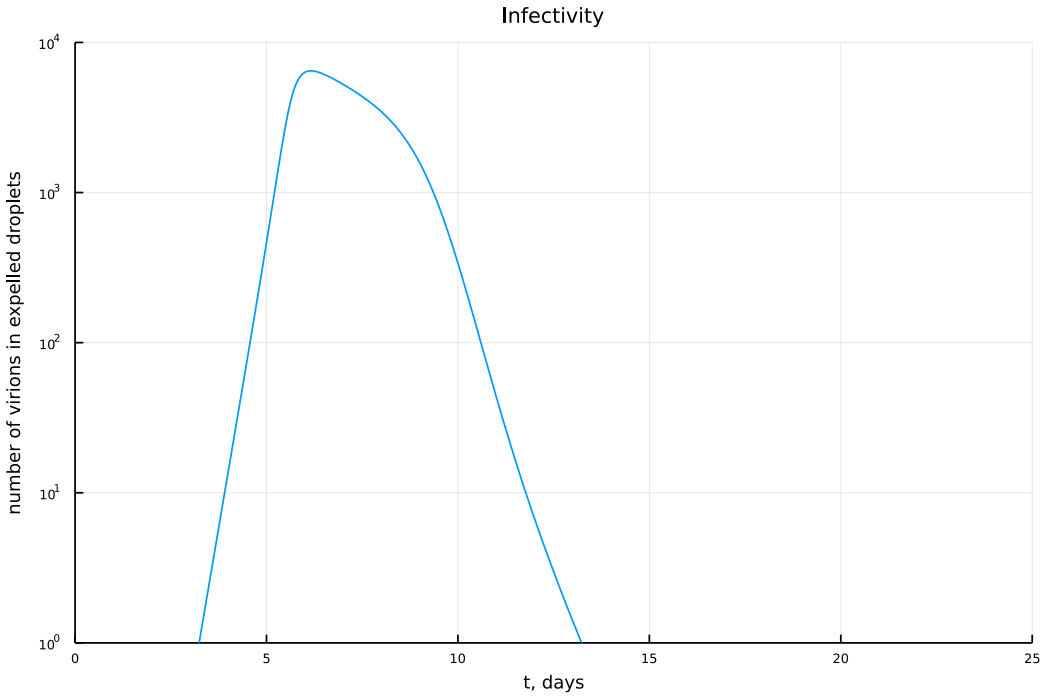

Figure 14. Kinetics of the number of virions in expelled droplets during the time course of infection.

Table 2. Thresholds for individual parameter variations which lead to virus persistence.

Parameter	γ_{MV}	b_p^P	b_p^B	b_p^E	b_H^B	b_H^E	γ_{M_I}	σ_R	μ_V	μ_C
Variation	$\div 1.12$	$\times 3$	$\div 1.4$	–	$\div 1.15$	–	$\times 1.15$	$\times 1.06$	$\times 1.3$	$\times 8 \times 10^4$

The model predicts that a 12%, 15% and 6% shift in the values of innate immune cells activation parameters, i.e. γ_{MV}, γ_{M_I}, σ_R respectively, turns out to be sufficient to extend the viral persistence beyond 30 days post infection. The robustness with respect to the B cell proliferation and differentiation shift is stronger. The inflammation-related enhancement of virus- and infected cell elimination parameters μ_V, μ_C is robust to 30% and 8×10^4-fold increase, respectively. 15% reduction of the activation rate of Th2 cells compared to Th1 cells results in prolonged virus persistence.

3.7. Individual's infectiousness

The kinetics of the viral load in upper respiratory tract reproduced by the model can be translated into the estimates of the number of viruses expelled by infected individual during talking via droplets [9]. Given the estimate of the volume of the expelled droplets $V_{droplets} = 1.1 \times 10^{-4}$ ml [9], we can obtain the number of expelled virions (infectiousness) as $V_{droplets} \times V(t)$. The time-course of an airborne transmission intensity of an infected person as predicted by the calibrated model is presented in Figure 14.

4. Discussion

In this study we developed a calibrated mathematical model of antiviral immune response to SARS-CoV-2 infection. Recently published data sets from the human challenge studies with SARS-CoV-2 were used for parameter estimation [22]. The model considers innate and antigen-specific responses to SARS-CoV-2 infection. In turn, the innate subsystem of equations describes the dynamics of the type I IFN responses and antigen presentation. The antigen specific immune response includes the clonal dynamics of Th1- and Th2 CD4 T cells, CD8 T cells, B cells, plasma cells and antibodies. The effect of inflammatory responses on elimination of the virus and infected cells is taken into account. The damage of the infected target cells (epithelial and endothelial cells, ciliated airway cells, alveoli type 2

cells) results in the suppression of antigen-specific immune responses. In our view, the model details provide an appropriate balance between the description of the complexity of SARS-CoV-2 infection and the consistency with the quantitative view of a mild-to-moderate symptoms COVID-19 [2,31,32,52].

Consideration of multiple immune reaction components in a single calibrated mathematical model allows one to address some fundamental issues related to the pathogenesis of COVID-19, e.g., sensitivity of peak viral load to parameters characterizing specific response components, the kinetic coordination of the individual responses, and factors favoring prolonged viral persistence.

Our model-based analyses suggest that the sequele of immune responses differentially mounted by innate and adaptive subsystems needs to be kinetically synchronized to ensure an optimal induction of the whole cascade. An improper increase of the activation rate of one single component may result into reduced responses of the others thus favouring the virus persistence. This observation corroborate results of the recent studies on age-related differences in immune dynamics in SARS-CoV-2 infection of non-human primates [46] and a delayed viral clearance in some asymptomatic human infections [47]. It was summarized that the major difference between the young and old rhesus macaques is a much stronger innate response and a delayed antigen-specific response in older animals [46]. The dysregulation of innate and adaptive immune responses was considered to result in a prolonged SARS-CoV-2 persistence [47].

The above finding bears a direct implication for a mechanistic understanding of prolonged viral persistence, i.e. beyond 30 days post infection. The problem of long-COVID-19 is emerging as a key pathological consequence of SARS-CoV-2 infection [43]. Although the set of etiological factors is very broad [44], the residual persistence of viral RNA is considered among them [48]. We identified the thresholds in the increase of the innate and adaptive responses parameters which lead to a prolonged persistence of SARS-CoV2 due to the loss of a kinetic synchrony/coordination of the responses, i.e. to the loss of an optimal pattern of their cascade.

Finally, the model can be used to predict the intensity of airborne infection spreading by infected individuals, e.g. the amount of virus which is transmitted via droplets from a SARS-CoV-2 infected person, depending on the time of infection and the immune response parameters. This type of estimates provide a direct information that may be included into the epidemiological models of virus spreading in the human population [49,53]. We note that a probabilistic model was recently elaborated linking the viral load and the host infectiousness [15]. It was used to evaluate the effectiveness of PCR and antigen-based testing.

The future development of the model will be related to a fine tuning of parameters and compartmental (multi-organ) extension of the equations to deal with the systemic aspects of COVID-19 [27,50]. A fundamental issue which remains to be explored is the incorporation of the regulatory feedbacks into the model, e.g., taking into account the pleiotropic effects of type I IFN, cytokines and networking of immune cells subsets. However, these refinements should go in coordination with clinical and experimental studies so that the increase of the model complexity could be justified.

Overall, our study highlights the value of mathematical modelling in gaining a mechanistic view of the kinetic regulations of SARS-CoV-2 infections and antiviral immune responses. It enables to draw novel hypotheses clarifying the concept of the 'numbers game' [51] or race between viral replication and activation of immune system arms [52], i.e., the kinetic coordination of multi-component immune reactions, on the course and outcome of COVID-19.

Author Contributions: Conceptualization, G.B., A.M. and D.G.; methodology, D.G., A.K., M.L., A.M. and G.B.; software, D.G.; validation, D.G., A.K., M.L., V.C., A.M. and G.B.; investigation, D.G. and G.B.; data curation, D.G., A.K., M.L., V.C., A.M. and G.B.; writing–review and editing, D.G., A.K., M.L., V.C., A.M. and G.B.; funding acquisition, A.M. and G.B.; All authors have read and agreed to the published version of the manuscript.

Funding: The reported study was funded by RFBR according to the research projects number 20-04-60157 and 20-01-00352. AM is also supported by the Spanish Ministry of Science and Innovation grant no. PID2019-106323RB-I00(AEI/MINEICO/FEDER, UE), and "Unidad de Excelencia María de Maeztu", funded by the AEI (CEX2018-000792-M).

Conflicts of Interest: The authors declare no conflict of interest. The funders had no role in the design of the study; in the collection, analyses, or interpretation of data; in the writing of the manuscript, or in the decision to publish the results.

Abbreviations

The following abbreviations are used in this manuscript:

SARS-CoV-2	Severe acute respiratory syndrome coronavirus
ODE	Ordinary differential equations
COVID-19	Infectious disease caused by SARS-CoV-2
IFN-I	type I interferon

References

1. Ostaszewski M, Niarakis A, Mazein A, Kuperstein I, Phair R, Orta-Resendiz A, Singh V, Aghamiri SS, Acencio ML, Glaab E, Ruepp A, Fobo G, Montrone C, Brauner B, Frishman G, Monraz Gómez LC, Somers J, Hoch M, Kumar Gupta S, Scheel J, Borlinghaus H, Czauderna T, Schreiber F, Montagud A, Ponce de Leon M, Funahashi A, Hiki Y, Hiroi N, Yamada TG, Dräger A, Renz A, Naveez M, Bocskei Z, Messina F, Börnigen D, Fergusson L, Conti M, Rameil M, Nakonecnij V, Vanhoefer J, Schmiester L, Wang M, Ackerman EE, Shoemaker JE, Zucker J, Oxford K, Teuton J, Kocakaya E, Summak GY, Hanspers K, Kutmon M, Coort S, Eijssen L, Ehrhart F, Rex DAB, Slenter D, Martens M, Pham N, Haw R, Jassal B, Matthews L, Orlic-Milacic M, Senff Ribeiro A, Rothfels K, Shamovsky V, Stephan R, Sevilla C, Varusai T, Ravel JM, Fraser R, Ortseifen V, Marchesi S, Gawron P, Smula E, Heirendt L, Satagopam V, Wu G, Riutta A, Golebiewski M, Owen S, Goble C, Hu X, Overall RW, Maier D, Bauch A, Gyori BM, Bachman JA, Vega C, Grouès V, Vazquez M, Porras P, Licata L, Iannuccelli M, Sacco F, Nesterova A, Yuryev A, de Waard A, Turei D, Luna A, Babur O, Soliman S, Valdeolivas A, Esteban-Medina M, Peña-Chilet M, Rian K, Helikar T, Puniya BL, Modos D, Treveil A, Olbei M, De Meulder B, Ballereau S, Dugourd A, Naldi A, Noël V, Calzone L, Sander C, Demir E, Korcsmaros T, Freeman TC, Augé F, Beckmann JS, Hasenauer J, Wolkenhauer O, Wilighagen EL, Pico AR, Evelo CT, Gillespie ME, Stein LD, Hermjakob H, D'Eustachio P, Saez-Rodriguez J, Dopazo J, Valencia A, Kitano H, Barillot E, Auffray C, Balling R, Schneider R; COVID-19 Disease Map Community. COVID19 Disease Map, a computational knowledge repository of virus-host interaction mechanisms. Mol Syst Biol. 2021 Oct;17(10):e10387. doi: 10.15252/msb.202110387. Erratum in: Mol Syst Biol. 2021 Dec;17(12):e10851. PMID: 34664389; PMCID: PMC8524328.
2. Bar-On YM, Flamholz A, Phillips R, Milo R. SARS-CoV-2 (COVID-19) by the numbers. Elife. 2020 Apr 2;9:e57309. doi: 10.7554/eLife.57309. PMID: 32228860; PMCID: PMC7224694.
3. Du SQ, Yuan W. Mathematical modeling of interaction between innate and adaptive immune responses in COVID-19 and implications for viral pathogenesis. J Med Virol. 2020 Sep;92(9):1615-1628. doi: 10.1002/jmv.25866.
4. Wang S, Pan Y, Wang Q, Miao H, Brown AN, Rong L. Modeling the viral dynamics of SARS-CoV-2 infection. Math Biosci. 2020 Oct;328:108438. doi: 10.1016/j.mbs.2020.108438.
5. Hernandez-Vargas EA, Velasco-Hernandez JX. In-host Mathematical Modelling of COVID-19 in Humans. Annu Rev Control. 2020;50:448-456. doi: 10.1016/j.arcontrol.2020.09.006.
6. Chimal-Eguia, J.C. Mathematical Model of Antiviral Immune Response against the COVID-19 Virus. Mathematics 2021, 9, 1356.
7. Rodriguez T, Dobrovolny HM. Estimation of viral kinetics model parameters in young and aged SARS-CoV-2 infected macaques. R Soc Open Sci. 2021 Nov 17;8(11):202345. doi: 10.1098/rsos.202345.
8. Sadria M, Layton AT. Modeling within-Host SARS-CoV-2 Infection Dynamics and Potential Treatments. Viruses. 2021 Jun 14;13(6):1141. doi: 10.3390/v13061141.
9. Fatehi F, Bingham RJ, Dykeman EC, Stockley PG, Twarock R. Comparing antiviral strategies against COVID-19 via multiscale within-host modelling. R Soc Open Sci. 2021 Aug 11;8(8):210082. doi: 10.1098/rsos.210082.
10. Voutouri C, Nikmaneshi MR, Hardin CC, Patel AB, Verma A, Khandekar MJ, Dutta S, Stylianopoulos T, Munn LL, Jain RK. In silico dynamics of COVID-19 phenotypes for optimizing clinical management. Proc Natl Acad Sci U S A. 2021 Jan 19;118(3):e2021642118. doi: 10.1073/pnas.2021642118.
11. Blanco-Rodríguez R, Du X, Hernández-Vargas E. Computational simulations to dissect the cell immune response dynamics for severe and critical cases of SARS-CoV-2 infection. Comput Methods Programs Biomed. 2021 Nov;211:106412. doi: 10.1016/j.cmpb.2021.106412.
12. Ghosh I. Within Host Dynamics of SARS-CoV-2 in Humans: Modeling Immune Responses and Antiviral Treatments. SN Comput Sci. 2021;2(6):482. doi: 10.1007/s42979-021-00919-8.

13. Jenner AL, Aogo RA, Alfonso S, Crowe V, Deng X, Smith AP, Morel PA, Davis CL, Smith AM, Craig M. COVID-19 virtual patient cohort suggests immune mechanisms driving disease outcomes. PLoS Pathog. 2021 Jul 14;17(7):e1009753. doi: 10.1371/journal.ppat.1009753. PMID: 34260666;
14. Mochan E, Sego TJ, Gaona L, Rial E, Ermentrout GB. Compartmental Model Suggests Importance of Innate Immune Response to COVID-19 Infection in Rhesus Macaques. Bull Math Biol. 2021 May 26;83(7):79. doi: 10.1007/s11538-021-00909-0.
15. Ke R, Zitzmann C, Ho DD, Ribeiro RM, Perelson AS. In vivo kinetics of SARS-CoV-2 infection and its relationship with a person's infectiousness. Proc Natl Acad Sci U S A. 2021 Dec 7;118(49):e2111477118. doi: 10.1073/pnas.2111477118.
16. Mondal J, Samui P, Chatterjee AN. Dynamical demeanour of SARS-CoV-2 virus undergoing immune response mechanism in COVID-19 pandemic. Eur Phys J Spec Top. 2022 Jan 20:1-14. doi: 10.1140/epjs/s11734-022-00437-5.
17. Rana P, Chauhan S, Mubayi A. Burden of cytokines storm on prognosis of SARS-CoV-2 infection through immune response: dynamic analysis and optimal control with immunomodulatory therapy. Eur Phys J Spec Top. 2022 Jan 27:1-19. doi: 10.1140/epjs/s11734-022-00435-7.
18. Marzban S, Han R, Juhász N, Röst G. A hybrid PDE-ABM model for viral dynamics with application to SARS-CoV-2 and influenza. R Soc Open Sci. 2021 Nov 3;8(11):210787. doi: 10.1098/rsos.210787.
19. Afonyushkin, V.N.; Akberdin, I.R.; Kozlova, Y.N.; Schukin, I.A.; Mironova, T.E.; Bobikova, A.S.; Cherepushkina, V.S.; Donchenko, N.A.; Poletaeva, Y.E.; Kolpakov, F.A. Multicompartmental Mathematical Model of SARS-CoV-2 Distribution in Human Organs and Their Treatment. Mathematics 2022, 10, 1925. https://doi.org/10.3390/math10111925
20. Getz M, Wang Y, An G, Asthana M, Becker A, Cockrell C, Collier N, Craig M, Davis CL, Faeder JR, Ford Versypt AN, Mapder T, Gianlupi JF, Glazier JA, Hamis S, Heiland R, Hillen T, Hou D, Islam MA, Jenner AL, Kurtoglu F, Larkin CI, Liu B, Macfarlane F, Maygrundter P, Morel PA, Narayanan A, Ozik J, Pienaar E, Rangamani P, Saglam AS, Shoemaker JE, Smith AM, Weaver JJA, Macklin P. Iterative community-driven development of a SARS-CoV-2 tissue simulator. bioRxiv [Preprint]. 2021 Nov 10:2020.04.02.019075. doi: 10.1101/2020.04.02.019075.
21. Alexandre M, Marlin R, Prague M, Coleon S, Kahlaoui N, Cardinaud S, Naninck T, Delache B, Surenaud M, Galhaut M, Dereuddre-Bosquet N, Cavarelli M, Maisonnasse P, Centlivre M, Lacabaratz C, Wiedemann A, Zurawski S, Zurawski G, Schwartz O, Sanders RW, Le Grand R, Levy Y, Thiébaut R. Modelling the response to vaccine in non-human primates to define SARS-CoV-2 mechanistic correlates of protection. Elife. 2022 Jul 8;11:e75427. doi: 10.7554/eLife.75427. PMID: 35801637; PMCID: PMC9282856.
22. Killingley B, Mann AJ, Kalinova M, Boyers A, Goonawardane N, Zhou J, Lindsell K, Hare SS, Brown J, Frise R, Smith E, Hopkins C, Noulin N, Löndt B, Wilkinson T, Harden S, McShane H, Baillet M, Gilbert A, Jacobs M, Charman C, Mande P, Nguyen-Van-Tam JS, Semple MG, Read RC, Ferguson NM, Openshaw PJ, Rapeport G, Barclay WS, Catchpole AP, Chiu C. Safety, tolerability and viral kinetics during SARS-CoV-2 human challenge in young adults. Nat Med. 2022 May;28(5):1031-1041. doi: 10.1038/s41591-022-01780-9. Epub 2022 Mar 31. PMID: 35361992.
23. Bocharov GA, Romanyukha AA. Mathematical model of antiviral immune response. III. Influenza A virus infection. J Theor Biol. 1994 Apr 21;167(4):323-60. doi: 10.1006/jtbi.1994.1074. PMID: 7516024.
24. Grossman Z, Paul WE. Dynamic tuning of lymphocytes: physiological basis, mechanisms, and function. Annu Rev Immunol. 2015;33:677-713. doi: 10.1146/annurev-immunol-032712-100027. Epub 2015 Feb 6. PMID: 25665077.
25. Bocharov G, Grebennikov D, Argilaguet J, Meyerhans A. Examining the cooperativity mode of antibody and CD8+ T cell immune responses for vaccinology. Trends Immunol. 2021 Oct;42(10):852-855. doi: 10.1016/j.it.2021.08.003. Epub 2021 Sep 21. PMID: 34561159.
26. Hou YJ, Okuda K, Edwards CE, Martinez DR, Asakura T, Dinnon KH 3rd, Kato T, Lee RE, Yount BL, Mascenik TM, Chen G, Olivier KN, Ghio A, Tse LV, Leist SR, Gralinski LE, Schäfer A, Dang H, Gilmore R, Nakano S, Sun L, Fulcher ML, Livraghi-Butrico A, Nicely NI, Cameron M, Cameron C, Kelvin DJ, de Silva A, Margolis DM, Markmann A, Bartelt L, Zumwalt R, Martinez FJ, Salvatore SP, Borczuk A, Tata PR, Sontake V, Kimple A, Jaspers I, O'Neal WK, Randell SH, Boucher RC, Baric RS. SARS-CoV-2 Reverse Genetics Reveals a Variable Infection Gradient in the Respiratory Tract. Cell. 2020 Jul 23;182(2):429-446.e14. doi: 10.1016/j.cell.2020.05.042. Epub 2020 May 27. PMID: 32526206; PMCID: PMC7250779.
27. Mettelman RC, Allen EK, Thomas PG. Mucosal immune responses to infection and vaccination in the respiratory tract. Immunity. 2022 May 10;55(5):749-780. doi: 10.1016/j.immuni.2022.04.013. PMID: 35545027; PMCID: PMC9087965.
28. Wiech M, Chroscicki P, Swatler J, Stepnik D, De Biasi S, Hampel M, Brewinska-Olchowik M, Maliszewska A, Sklinda K, Durlik M, Wierzba W, Cossarizza A, Piwocka K. Remodeling of T Cell Dynamics During Long COVID Is Dependent on Severity of SARS-CoV-2 Infection. Front Immunol. 2022 Jun 10;13:886431. doi: 10.3389/fimmu.2022.886431.
29. Zuin J, Fogar P, Musso G, Padoan A, Piva E, Pelloso M, Tosato F, Cattelan A, Basso D, Plebani M. T Cell Senescence by Extensive Phenotyping: An Emerging Feature of COVID-19 Severity. Lab Med. 2022 Jun 18:lmac048. doi: 10.1093/labmed/lmac048. Epub ahead of print.
30. Grebennikov D, Kholodareva E, Sazonov I, Karsonova A, Meyerhans A, Bocharov G. Intracellular Life Cycle Kinetics of SARS-CoV-2 Predicted Using Mathematical Modelling. Viruses. 2021 Aug 31;13(9):1735. doi: 10.3390/v13091735. PMID: 34578317; PMCID: PMC8473439.
31. Tan AT, Linster M, Tan CW, Le Bert N, Chia WN, Kunasegaran K, Zhuang Y, Tham CYL, Chia A, Smith GJD, Young B, Kalimuddin S, Low JGH, Lye D, Wang LF, Bertoletti A. Early induction of functional SARS-CoV-2-specific T cells associates with rapid viral clearance and mild disease in COVID-19 patients. Cell Rep. 2021 Feb 9;34(6):108728. doi: 10.1016/j.celrep.2021.108728. Epub 2021 Jan 21. PMID: 33516277; PMCID: PMC7826084.

32. Cheemarla NR, Watkins TA, Mihaylova VT, Wang B, Zhao D, Wang G, Landry ML, Foxman EF. Dynamic innate immune response determines susceptibility to SARS-CoV-2 infection and early replication kinetics. J Exp Med. 2021 Aug 2;218(8):e20210583. doi: 10.1084/jem.20210583. Epub 2021 Jun 15. PMID: 34128960; PMCID: PMC8210587.
33. Zinkernagel RM, Hengartner H. On immunity against infections and vaccines: credo 2004. Scand J Immunol. 2004 Jul-Aug;60(1-2):9-13. doi: 10.1111/j.0300-9475.2004.01460.x. Erratum in: Scand J Immunol. 2004 Sep;60(3):327.
34. Janeway's Immunobiology. 9th Edition. By Kenneth Murphy, Casey Weaver. Published March 1, 2017. Garland Science, Taylor and Francis Group, LLC. 924 Pages. ISBN 978-0-8153-4505-3.
35. Deem MW, Hejazi P. Theoretical aspects of immunity. Annu Rev Chem Biomol Eng. 2010;1:247-76. doi: 10.1146/annurev-chembioeng-073009-100952.
36. Perelson A.S., Weisbuch G. Immunology for physicists. Rev. Mod. Phys. 1997, 69(4): 1219–1268. doi: 10.1103/RevModPhys.69.1219.
37. Cosgrove J, Hustin LSP, de Boer RJ, Perié L. Hematopoiesis in numbers. Trends Immunol. 2021 Dec;42(12):1100-1112. doi: 10.1016/j.it.2021.10.006. Epub 2021 Nov 3.
38. Sazonov I, Grebennikov D, Meyerhans A, Bocharov G. Sensitivity of SARS-CoV-2 Life Cycle to IFN Effects and ACE2 Binding Unveiled with a Stochastic Model. Viruses. 2022; 14(2):403. https://doi.org/10.3390/v14020403
39. Beule, A.G. Physiology and Pathophysiology of Respiratory Mucosa of the Nose and the Paranasal Sinuses. GMS Current Topics in Otorhinolaryngology - Head and Neck Surgery; 9:Doc07; ISSN 1865-1011 2010, doi:10.3205/CTO000071.
40. Ritthidej, G.C. Nasal Delivery of Peptides and Proteins with Chitosan and Related Mucoadhesive Polymers. In Peptide and Protein Delivery; Elsevier, 2011; pp. 47–68 ISBN 9780123849359.
41. Skevaki C, Karsonova A, Karaulov A, Fomina D, Xie M, Chinthrajah S, Nadeau KC, Renz H. SARS-CoV-2 infection and COVID-19 in asthmatics: a complex relationship. Nat Rev Immunol. 2021 Apr;21(4):202-203. doi: 10.1038/s41577-021-00516-z. PMID: 33623123; PMCID: PMC7901163.
42. Vabret N, Britton GJ, Gruber C, Hegde S, Kim J, Kuksin M, Levantovsky R, Malle L, Moreira A, Park MD, Pia L, Risson E, Saffern M, Salomé B, Esai Selvan M, Spindler MP, Tan J, van der Heide V, Gregory JK, Alexandropoulos K, Bhardwaj N, Brown BD, Greenbaum B, Gümüş ZH, Homann D, Horowitz A, Kamphorst AO, Curotto de Lafaille MA, Mehandru S, Merad M, Samstein RM; Sinai Immunology Review Project. Immunology of COVID-19: Current State of the Science. Immunity. 2020 Jun 16;52(6):910-941. doi: 10.1016/j.immuni.2020.05.002. Epub 2020 May 6. PMID: 32505227; PMCID: PMC7200337.
43. Couzin-Frankel J. Clues to long COVID. Science. 2022 Jun 17;376(6599):1261-1265. doi: 10.1126/science.add4297.
44. Peluso MJ, Deeks SG. Early clues regarding the pathogenesis of long-COVID. Trends Immunol. 2022 Apr;43(4):268-270. doi: 10.1016/j.it.2022.02.008. Epub 2022 Mar 8. PMID: 35272932; PMCID: PMC8901423.
45. Su Y, Yuan D, Chen DG, Ng RH, Wang K, Choi J, Li S, Hong S, Zhang R, Xie J, Kornilov SA, Scherler K, Pavlovitch-Bedzyk AJ, Dong S, Lausted C, Lee I, Fallen S, Dai CL, Baloni P, Smith B, Duvvuri VR, Anderson KG, Li J, Yang F, Duncombe CJ, McCulloch DJ, Rostomily C, Troisch P, Zhou J, Mackay S, DeGottardi Q, May DH, Taniguchi R, Gittelman RM, Klinger M, Snyder TM, Roper R, Wojciechowska G, Murray K, Edmark R, Evans S, Jones L, Zhou Y, Rowen L, Liu R, Chour W, Algren HA, Berrington WR, Wallick JA, Cochran RA, Micikas ME; ISB-Swedish COVID-19 Biobanking Unit, Wrin T, Petropoulos CJ, Cole HR, Fischer TD, Wei W, Hoon DSB, Price ND, Subramanian N, Hill JA, Hadlock J, Magis AT, Ribas A, Lanier LL, Boyd SD, Bluestone JA, Chu H, Hood L, Gottardo R, Greenberg PD, Davis MM, Goldman JD, Heath JR. Multiple early factors anticipate post-acute COVID-19 sequelae. Cell. 2022 Mar 3;185(5):881-895.e20. doi: 10.1016/j.cell.2022.01.014. Epub 2022 Jan 25. PMID: 35216672; PMCID: PMC8786632.
46. Speranza E, Purushotham JN, Port JR, Schwarz B, Flagg M, Williamson BN, Feldmann F, Singh M, Pérez-Pérez L, Sturdevant GL, Roberts LM, Carmody A, Schulz JE, van Doremalen N, Okumura A, Lovaglio J, Hanley PW, Shaia C, Germain RN, Best SM, Munster VJ, Bosio CM, de Wit E. Age-related differences in immune dynamics during SARS-CoV-2 infection in rhesus macaques. Life Sci Alliance. 2022 Jan 17;5(4):e202101314. doi: 10.26508/lsa.202101314. PMID: 35039442; PMCID: PMC8807873.
47. Cao S, Zhang Q, Song L, Xiao M, Chen Y, Wang D, Li M, Hu J, Lin L, Zheng Y, Zhou K, Ye S, Zhou J, Zhou YN, Cui J, Wang J, Sun J, Tao J, Chen Z, Chen R, Zhou P, Shi Z, Wei S, Zhao L, Wang H, Tong X, Li X, Men D, Hou B, Zhang XE. Dysregulation of Innate and Adaptive Immune Responses in Asymptomatic SARS-CoV-2 Infection with Delayed Viral Clearance. Int J Biol Sci. 2022 Jul 11;18(12):4648-4657. doi: 10.7150/ijbs.72963.
48. Manthiram K, Xu Q, Milanez-Almeida P, Martins A, Radtke A, Hoehn K, Chen J, Liu C, Tang J, Grubbs G, Stein S, Ramelli S, Kabat J, Behzadpour H, Karkanitsa M, Spathies J, Kalish H, Kardava L, Kirby M, Cheung F, Preite S, Duncker P, Romero N, Preciado D, Gitman L, Koroleva G, Smith G, Shaffer A, McBain I, Pittaluga S, Germain R, Apps R, Sadtler K, Moir S, Chertow D, Kleinstein S, Khurana S, Tsang J, Mudd P, Schwartzberg P. Robust, persistent adaptive immune responses to SARS-CoV-2 in the oropharyngeal lymphoid tissue of children. Res Sq [Preprint]. 2022 Mar 23:rs.3.rs-1276578. doi: 10.21203/rs.3.rs-1276578/v1. PMID: 35350206; PMCID: PMC8963700.
49. Wadman M, Couzin-Frankel J, Kaiser J, Matacic C. A rampage through the body. Science. 2020 Apr 24;368(6489):356-360. doi: 10.1126/science.368.6489.356. PMID: 32327580.
50. Simoneau CR, Ott M. Modeling Multi-organ Infection by SARS-CoV-2 Using Stem Cell Technology. Cell Stem Cell. 2020 Dec 3;27(6):859-868. doi: 10.1016/j.stem.2020.11.012. PMID: 33275899; PMCID: PMC7713543.
51. Zinkernagel RM, Hengartner H, Stitz L. On the role of viruses in the evolution of immune responses. Br Med Bull. 1985 Jan;41(1):92-7. doi: 10.1093/oxfordjournals.bmb.a072033. PMID: 3882192.
52. Raoult D, Zumla A, Locatelli F, Ippolito G, Kroemer G. Coronavirus infections: Epidemiological, clinical and immunological features and hypotheses. Cell Stress. 2020 Mar 2;4(4):66-75. doi: 10.15698/cst2020.04.216. PMID: 32292881; PMCID: PMC7064018.

53. Pertsev N., Loginov K., Lukashev A., Vakulenko Yu. Stochastic Modeling of Dynamics of the Spread of COVID-19 Infection Taking Into Account the Heterogeneity of Population According To Immunological, Clinical and Epidemiological Criteria. Math. Biol. Bioinf. 2022;17(1):43-81 doi: 10.17537/2022.17.43 (published in Russian)